UNIVERSITY OF AGDER

Modelling of a Hydro-Pneumatic system for Heave Compensation

John Kenneth Hatletvedt

Supervisor
Jing Zhou
Alf Kristian Gjerstad

This Master's Thesis is carried out as a part of the education at the

University of Agder and is therefore approved as a part of this education. However, this does not imply that the University answers for the methods that are used or the conclusions that are drawn.

University of Agder, 2018
Faculty of Engineering and Science
Department of Engineering Sciences

Acknowledgement

I would like to thank MHWirth which has provided me with an exciting thesis.
I would especially thank my supervisor at MHWirth, Kristian Gjerstad, who always had an answer to my questions.

I would also like to thank my supervisor at the University, Jing Zhou.

At last, I would like to thank for the support and answers from Christian H. Andersen at the office in Horten.

Abstract

Testing of control systems on simulators has been found to be both cost and time efficient. To get good results from testing, a realistic response from the simulator is important. In this thesis, a mathematical model of a hydro-pneumatic heave compensation system for such purposes is proposed. The emphasis has been on developing a relatively simple model which is easy to run, but also accounts for important effects like friction, non-ideal gas behaviour and temperature variation in the gas system.

The mathematical model is verified against log data obtained from real drilling operations. Then, it is compared to simpler versions to investigate and discuss the importance of including temperature variation and non-ideal gas behaviour.

It was found that the model was in good accordance with the log data. When neglecting the temperature variation, a deviation in pressure variation of 20-30% from the original model was experienced. For the given conditions, a deviation of about 4% from non-ideal gas equations was found when assuming ideal gas. This is in good accordance with the compressibility chart. To verify the deviations found in the compressibility chart, a simulation closer to the critical point was performed. It was concluded that the compressibility chart should be used as an indication of the applicability, and accuracy obtained, under the assumption of the ideal gas in this model.

Contents

List of Figures

Chapter 1

Introduction

High technical level, high production costs and small production numbers are a well-known fact for participants in the oil and gas industry. Creating prototypes for testing and evaluating new designs are time consuming, and thus a big expense for the manufacturer. Lately, there have been an increased focus on tools for virtual prototyping and simulations of new design. These tools make it possible for engineers to test, adjust and optimize their design before manufacturing it. This leads to lower cost for the manufacturer. It can also indirectly lower the risk for personnel working with the equipment by detecting critical faults or malfunctioning components in the design stage [5].

To meet the demands of the current state of the industry, MHWirth is interested to further develop the modeling and simulation of their systems. Dynamic models of a system can be used in a big variety of applications, such as simulator training, model prediction and Hardware-In-The-Loop (HIL) Testing. The latter is a relatively new approach but has proved to be a very efficient way of testing and verifying new designs [6]. The big advantage of HIL testing is that it emulates the actual system in real time, meaning that the actual hardware and software response can be tested in a more realistic way without having to mount it on the actual system. This has proven to be both time and cost effective.
When modelling complex systems the model often ends up requiring a lot of computational effort. These models provide good and accurate results, but at the cost of simulation time. The challenge is to make the models simpler, without loosing substantial accuracy.

1.1 Problem description

MHWirth delivers various heave compensation systems and associated control systems. For testing of control systems it is desirable to have mathematical models of the physical systems. In this project, which will be focusing on a crown mounted compensation system, the hydro-pneumatic part of the passive system is to be considered.

It is desirable to make a more detailed model which accounts for the temperature variation and the dynamics of the gas flow between the accumulator and APVs. It is also desirable to investigate if there is a significant difference in assuming non-ideal gas.
The pneumatic system is driven by the plunger piston in the hydraulic system. To get as realistic results as possible, the hydraulic system should be modelled, and interact with the pneumatic system.

1.2 Thesis overview

More details of the work contained in this thesis and a brief outline of the following chapters is now presented.

In *Chapter 2*, some theoretical background and equations will be presented. Background on heave compensation is given, before a thorough description of the heave compensation system under consideration in this thesis is given. A quick review of some basic thermodynamics is included, and literature regarding equations of state is presented. Governing equations for fluid dynamics used in chapter 3 is presented.

Chapter 3 goes in detail on the modelling of the system. The chapter is divided into a hydraulics part and a pneumatics part.

Chapter 4 presents results and plots obtained when simulating the model described in chapter 3. The model is first compared to log data, before different scenarios are tested and compared. Results and remarks about the behaviour will be discussed.

Lastly, *Chapter 5* will conclude the thesis, and contains conclusion and a summary of the findings from chapter 4. The chapter also contains some notes and recommendations for further work.

Chapter 2

Theory

2.1 Heave Compensation

On a floating rig, ocean waves will induce a vertical motion to the rig. As the rig heaves, this will put a lot of strain on the drill bit. To counteract this motion, heave compensators are mounted on the rigs. The goal of the heave compensation is to decouple the load motion from the ship motion [1]. This will keep a more constant weight on the drill bit, preventing excessive wear and tear during rough weather conditions.

There are two main categories for heave compensation: *passive* heave compensation, and *active* heave compensation. Additionally, there are also possibilities for a hybrid active-passive system, which combines the feature of the two systems.

2.1.1 Passive Heave Compensation

There are two different types of passive heave compensators: the crown mounted, which is mounted on top of the derrick, and the in-line compensator, which is placed below the travelling block [7].
The passive systems aims to be a flexible joint between the drilling machine and the rig. In passive systems, it is common to use a variation of a gas accumulator connected to a hydraulic driven piston, as is illustrated in figure 2.1. Here, the drilling equipment (load) will be attached to the piston, which is connected to an accumulator. The accumulator will be connected to the hydraulic system on one side, while the other side will consist of pressurized gas. As the hydraulic fluids enter the accumulator, and causing a rise in pressure, the gas will compress, acting like a flexible gas-spring.
The advantages with this system is that it needs no input energy, and there is no need for a control system to actively regulate the system. This makes it relatively simple in its construction, and troubleshooting on such systems

is an easy job compared to the active systems. The main drawback with the passive system is its accuracy. The passive systems will not be as accurate as the active systems, where there are control systems actively regulating the system at all times.

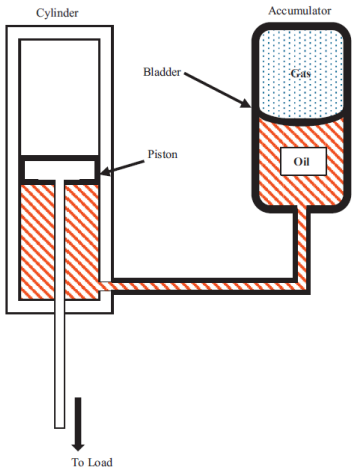

Figure 2.1: Simple sketch of the working principles of a passive heave compensation system [1]

2.1.2 Active Heave Compensation

Active systems are driven by an energy input and a control system constantly reacting to real time data provided from sensors. Often these systems requires high energy input and accurate control, which involves high cost machinery and software.
Active compensation is most commonly performed by hydraulic cylinders or by winch systems. In the case of hydraulic cylinders, the drilling equipment will be attached to a piston, based on the same principle as in passive compensation. Instead of connecting the cylinder to an accumulator, the pressure is controlled by pumping hydraulic fluid in and out of the cylinder, based on signals from the MRU. For heavy loads, this often includes high flow levels, and need to be accurately controlled. This concept is shown in figure 2.2.

Winch systems, often referred to as drawworks, are also used for active compensation. In these systems, wave movements are compensated by driving a winch in opposite direction of the heave motion. By doing this, the hook will keep a constant position relative to the sea bed. Signals from the MRU are being fed to a control system, regulating the speed and direction of a wire drum. The drum may be driven by either hydraulic or electric power.

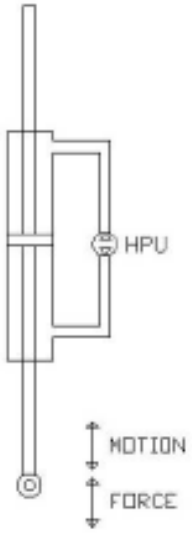

Figure 2.2: Hydraulic Active Heave Compensation Cylinder [2]

2.1.3 Crown Mounted Compensator

This section will give a description of the CMC system in focus for this thesis. The next chapter gives a detailed description of the mathematical modelling of this system.

MHWirth has developed a Crown Mounted heave Compensation (CMC) system found on various drilling rigs. This is a semi-active system which can operate with only the passive system activated, or together with an active system. A schematic of the passive system is shown in figure 2.3, and this can be divided into two subsystems: the hydraulic system and the pneumatic system. The hydraulic system is marked with green in this figure, and the pneumatic system is marked with blue.

The main driver of the compensation system is the plunger piston. Plunger pistons are single acting pistons with relatively thick rods, and are only able to exert force in one direction. The piston is located inside the plunger cylinder (3), which contains only one chamber and is filled with hydraulic oil. The hydraulic pressure will act on the bottom of the plunger piston, making the piston exert a "pushing" force upwards on the crown block. The weight of the drilling equipment attached to the crown block ensures retraction of the piston. As the piston retracts, hydraulic fluid will flow into the

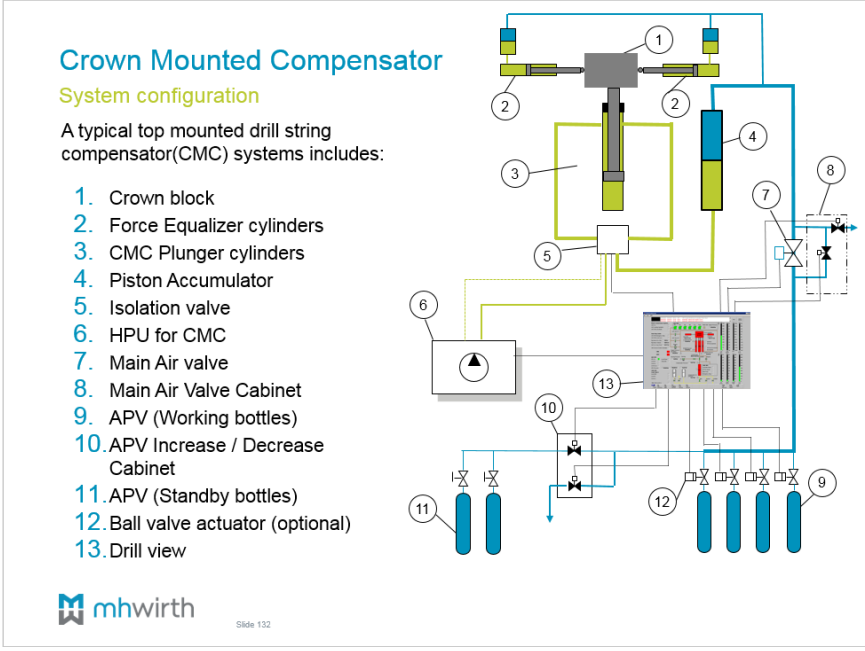

Figure 2.3: System configuration CMC

accumulator. The accumulator separates the hydraulics from the pneumatics, and as the hydraulic liquid flows into the accumulator, the piston in the accumulator will cause a change in pressure in the pneumatic system.
Between the plunger cylinder and the accumulator there is fitted an isolation valve. This valve makes it possible to isolate the plunger cylinder from the accumulator, and prevent the pistons from moving. The valve is equipped with a safety feature which automatically isolates the systems to prevent damage to personnel and equipment in case of a drill string break.

The pneumatic system consists of the accumulator(4), valve(7), air piping and Air Pressure Vessles (APVs)(9)(11). As the pressure in the accumulator changes, gas will flow between the accumulator and APVs. APVs are a series of connected gas bottles, providing additional volume for the flow to enter from the gas pipes. The APVs are divided into two groups: working bottles and standby bottles. The working bottles are supplying the additional volume. There are several bottles connected, making it possible to vary the total volume of the working APVs. Greater volume will decrease the stiffness of the system, as the pressure change will be more gradual. Varying the total volume can be viewed as the equivalent of changing the spring stiffness coefficient for a conventional mechanical spring. The standby APVs provide gas volumes of higher pressure than the working APVs. This allows for an instant pressure increase by bleeding gas from the standby

APVs to the working APVs if needed.
A valve(7) is fitted between the accumulator and APVs, and can vary the flow rate between the volumes. This will act as a flow restriction, and together with friction in the pipe walls, this will act as a natural damper for the system.

On top of the system there are located two force equalizer cylinders(2) which are designed to reduce the load variation over the complete piston stroke. As can be seen in the figure, the pressure in these cylinders depends on the pressure in the pneumatic system. Based on the position of the plunger piston, the pressure in the pneumatic system will vary, causing a change in pressure for the force equalizer cylinders. From log data it is found that the force exerted from the force equalizers on the crown block varies almost linearly with the plunger position for most of the piston stroke. This is illustrated in figure 2.4. In figure 2.4, the vertical force component relative to the total force acting on the crown block is plotted on the y-axis. The plunger position is plotted on the x-axis.

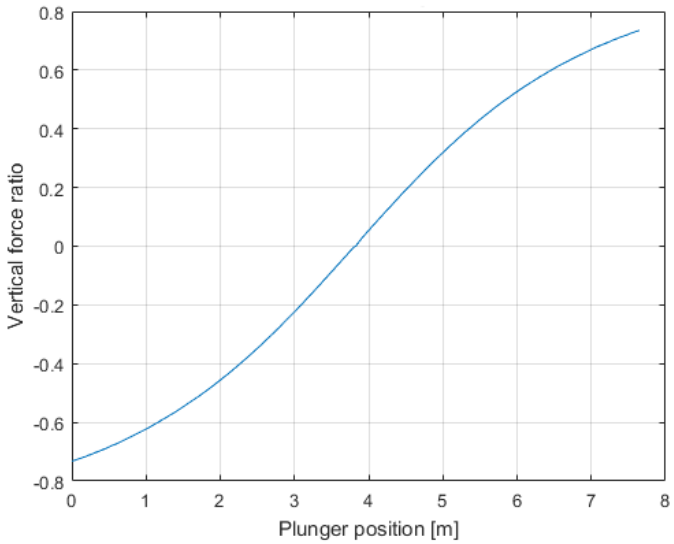

Figure 2.4: Vertical force ratio vs. plunger position

2.2 Thermodynamics

2.2.1 p-v-t relation and critical properties

Nitrogen is used as gas in the pneumatic system. When dealing with gas, thermodynamic considerations will come in to play sooner or later. The reader should be acquainted with some of the thermodynamic properties,

and they will be reviewed in short in this section.

In calculation of gas systems and other thermodynamic systems, an accurate representation of pressure, specific volume and temperature is important. These properties are used to define states and calculate other properties. In thermodynamics, this relation appears so often that it is commonly referred to as the *p-v-t relation.*

Most substances have three phases: solid, liquid and vapor, and most fluids change phases under some given conditions. The general behaviour can be illustrated on a p-v-t surface diagram, as depicted in figure 2.5.

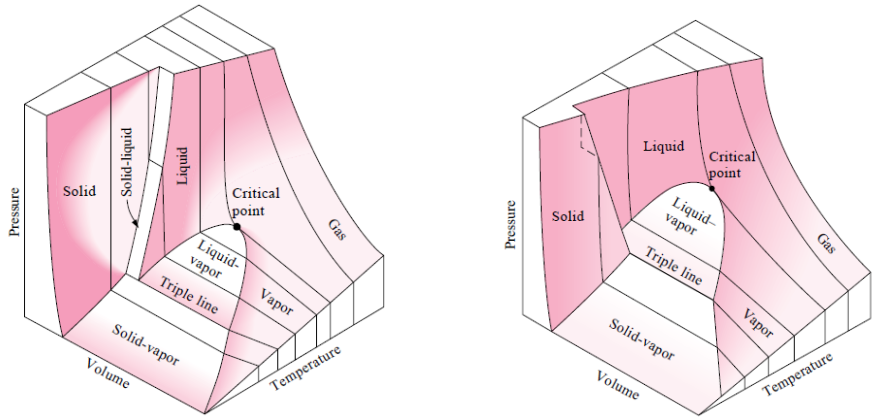

(a) p-v-t surface of a substance that contracts on freezing

(b) p-v-t surface of a substance that expands on freezing

Figure 2.5: p-v-t surface diagram [3]

This diagram shows the relation between solids, liquids and vapors. The regions show where the substance is in a *single-phase*, meaning that the state is fixed by any *two* of the properties: pressure, temperature and specific volume, since all of these properties are independent in single-phase. Between the single-phase regions are the *two-phase regions.* Here, two phases can co-exist in equilibrium, such as liquid-vapor, solid-liquid or solid-vapor. Within the two-phase regions, temperature and pressure are not independent. This means that the state cannot be fixed by pressure and temperature alone, and the specific volume is needed together with *either* pressure or temperature to fix the state. Along the *triple line* in the diagram, also three phases can co-exist in equilibrium.

The *critical point* in figure 2.5 is the point where saturated liquid lines and saturated vapor lines meet. This point defines the critical temperature T_{cr}, critical pressure p_{cr}, and critical specific volume $V_{m,cr}$. The critical temper-

ature is the maximum temperature at which liquid and vapor phases can coexist. Over this temperature it is not possible to liquefy gas/vapor. The critical pressure is the pressure required to liquefy gas at the critical temperature. The critical specific volume would be the specific volume at the critical point. Most substances encountered will have given critical properties which can be found in tables [8]. For a more thorough review of these concepts, the reader are referred to textbooks in thermodynamics, such as [8] or [3].

2.2.2 Equation of State (EOS)

There are many different ways of representing the p-v-t relation, such as tabular representation or graphical representation. Another, very common method, is by use of analytical formulation of the p-v-t relation. This is formulated by means of equations and are called equation of states (EOS). The equation of states are particularly convenient for performing mathematical operations required to calculate different thermodynamic properties [8].
One of the most basic equation of state has to be the ideal gas law. This law was defined in 1802 by Charles and Gay-Lussac, based on the findings of Boyle, all the way back in 1662 [3]. This law states that pressure is proportional to temperature, and inversely proportional to its volume, and is defined as

$$pV_m = RT \tag{2.1}$$

where
p = pressure
V_m = specific volume (volume per mass)
R = gas constant
T = temperature
This equation of state is frequently used in engineering practice due to its simplicity and it is convenient to use. The ideal gas law can give good prediction for the behaviour of gases, but it also has its limitations. The equation is most accurate for low pressures and high temperatures, and should not be used near saturation regions and near critical points [3].

To get a quick estimate for how much a gas will deviate from the ideal gas law, a correction factor called the compressibility factor can be used. This is usually denoted with a Z, and is defined as

$$Z = \frac{pV_m}{RT}. \tag{2.2}$$

For ideal gases, the compressibility factor will be 1. The farther away the compressibility factor is from unity, the more the gas will deviate from ideal behaviour.

Gases behave differently at given temperatures and pressures, but they are found to behave in similar fashions if normalized with respect to their critical temperatures and pressures [8]. Therefore, quantities called *reduced* pressure and temperature, p_R and T_R respectively, are defined:

$$p_R = \frac{p}{p_{cr}} \tag{2.3}$$

$$T_R = \frac{T}{T_c r}. \tag{2.4}$$

A lot of experiments has been done to obtain empirical values for the compressibility factor for different gases. By plotting these Z-values against p_R and T_R, and by curve-fitting the data, the generalized compressibility chart is obtained. This chart can be seen in figure 2.6.

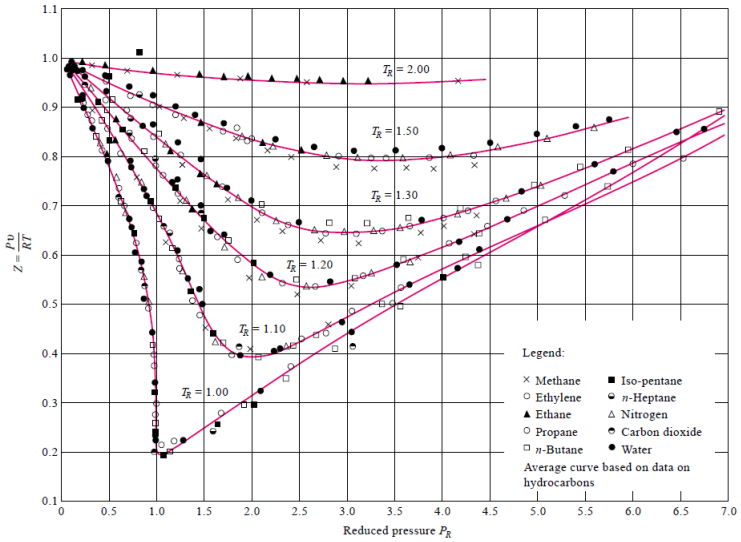

Figure 2.6: Generalized compressibility chart [3]

Research has shown that this chart gives good estimations for gas behaviour under different conditions [3].

During the years there have been a lot of research on different equations of state, and there are formulated hundreds of different EOS' [8], [4]. The equations are divided into different classes, like complex molecular-based equations, empirical multiparameter equations, virial equations, which is based on series expansion, cubic and higher order equations, and so on. Valderrama has made an overview over the most common classes of EOS', which can be seen in figure 2.7.
One of the most important improvements over the ideal gas law was stated by Van der Waals in 1873. The ideal gas law assumes that the gas molecules

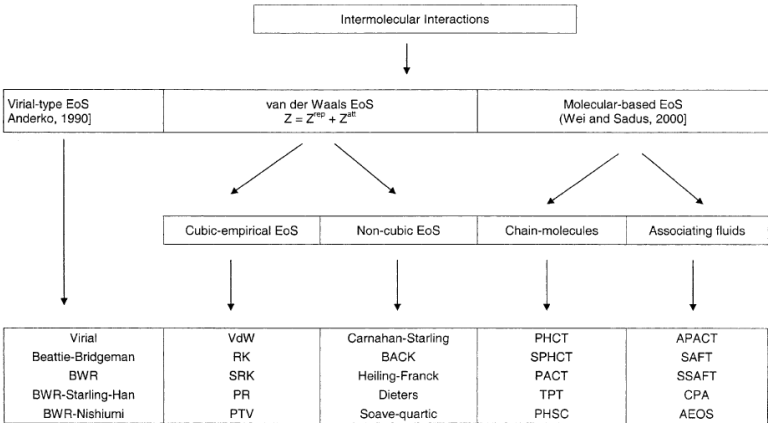

Figure 2.7: Different classes of EOS [4]

occupy a small and negligible volume, and that there is no intermolecular forces. Van der Waals noted that in many cases, this assumption would not be applicable. He stated a new equation of state where these phenomena are accounted for:

$$p = \frac{RT}{V_m - b} - \frac{a}{V_m^2} \tag{2.5}$$

where b is a constant and is intended to account for the finite volume occupied by the molecules, and the term $\frac{a}{v_m^2}$ accounts for the attraction forces between the molecules, with a being a constant to be determined.

Later, there has been proposed many improvements to this equation, all with different uses. The most common equations encountered in the petroleum industry are the Redlich-Kwong and Peng-Robinson equations of state [9]. The Redlich-Kwong EOS is a cubic equation based on the Van der Waals equation, and given as

$$p = \frac{RT}{V_m - b} - \frac{a}{\sqrt{T} V_m (V_m + b)} \tag{2.6}$$

with

$$a = 0.42748 \frac{R^2 T_c^{2.5}}{p_c}$$

$$b = 0.08664 \frac{RT_c}{p_c}$$

This equation improved the Van der Waals equation by finding a better description for the attractive term a, which accounted for temperature dependency. The main advantage of the Redlich-Kwong equation is its simplicity, and a greater accuracy than the Van der Waals equation. One of the disadvantages with the Redlich-Kwong equation is that it poorly predicts vapour

and liquid behaviour.

As an improvement of the Redlich-Kwong equation, Soave proposed a modification to the equation which fitted experimental vapor-liquid data. The modification involved making the attractive factor dependent on the acentric factor, ω, which is accounting for the shape of the gas molecules. The Soave-Redlich-Kwong equation can accurately describe both liquid and vapour phase behaviour, and is given as

$$p = \frac{RT}{V_m - b} - \frac{a\alpha}{V_m(V_m + b)} \tag{2.7}$$

where

$$\alpha = (1(0.480 + 1.574\omega - 0.176\omega^2(1 - \sqrt{T_R}))^2 \tag{2.8}$$

A major drawback for the Soave-Redlich-Kwong equation is the poor liquid density prediction.

The Peng-Robinson equation is a further improvement of the Soave-Redlich-Kwong equation. This equation and was developed to handle gas and condensate system, where the liquid density of the condensate is important. Peng and Robinson used the Soave-Redlich-Kwong equation, but also introduced various fitting parameters to describe the dependency of temperature and the acentric factor. The equation is given as

$$p = \frac{RT}{V_m - b} - \frac{a\alpha}{V_m(V_m + b) + b(b - V_m)} \tag{2.9}$$

with
$a = 0.45724\frac{R^2T_c^2}{p_c}$
$b = 0.07780\frac{RT_c}{p_c}$
$\alpha = 1 - \kappa(1 - T_R^{0.5}))^2$
$\kappa = 0.37464 + 1.54226\omega - 0.26992\omega^2$

In an article by Ramdharee et al. [9], the authors has compared the performance of these three equations. They found that the Redlich-Kwong equation can satisfactorily be applied to calculate gas phase properties and behaviour. The equation poorly predicted the liquid phase properties, so here one should use the Soave-Redlich-Kwong or Peng-Robinson equations. It was further found that for gas and condensate systems, often found in the natural gas system, the Peng-Robinson equation performed better compared to the Soave-Redlich-Kwong equation.
As highlighted in this section , there are a lot of different equations of state, and which equation to use should depend on application.

2.3 Fluid Dynamics

When solving fluid mechanics problems, it is common to use the conservation laws. These equations can found in almost all textbooks on basic fluid mechanics. This section will give a short introduction to the governing equations used in chapter 3, based on these laws.

2.3.1 Conservation of Mass

Consider a volume V, bounded by the surface area A, as shown in figure 2.8. The mass inside the volume, on a macroscopic basis, is given by $\int_V \rho \, dV$. Mass is a conserved property, and cannot be created or destroyed [3]. This means that the change in mass for a given volume must equal the flow of mass into the volume, minus the flow out of the volume.

Figure 2.8: Flow in a volume

The rate of mass flux across the surface a is given by $\rho \, v \cdot dA$. Integrating over the total volume gives the equation of conservation of mass as

$$\frac{d}{dt}\int_V \rho \, dV = \int_{A_{in}} \rho_{in} v_{in} \, dA_{in} - \int_{A_{out}} \rho_{out} v_{out} \, dA_{out} \tag{2.10}$$

As the density is assumed constant over the cross sectional area, this can be put outside of the integral. The remaining terms inside the integral can be identified as the volumetric flow rate. This gives the equation

$$\frac{d}{dt}(\rho V) = \rho_{in} Q_{in} - \rho_{out} Q_{out} \tag{2.11}$$

Notice that the volume V, may change if the boundaries of the control volume changes. Rearranging gives an expression explicit in density:

$$\frac{d\rho}{dt} = \frac{1}{V}\left(\rho_{in} Q_{in} - \rho_{out} Q_{out} - \rho \frac{dV}{dt}\right) \tag{2.12}$$

2.3.2 Conservation of Momentum

Consider a part of a conduit, with fluid flowing in it. Let the velocity, v, in x direction be constant in the z direction. This is referred to as a narrow slot

approximation [10]. If a one-dimensional flow is assumed, the conservation of momentum is given as

$$\rho\frac{\partial v}{\partial t} + \rho v\frac{\partial v}{\partial x} = -\frac{\partial p}{\partial x} + \frac{\partial \tau_{xx}}{\partial x} + \frac{\partial \tau_{yx}}{\partial y} \tag{2.13}$$

where p is pressure, and τ_{ij} is the shear stress in direction j, acting on the surface perpendicular to direction i.
As in the previous section, the density is assumed constant in space for the volume. The cross-sectional area A_p is constant, meaning that the flow velocity is constant over x, and the normal tension goes to zero. With these assumptions, a simplified equation can be set up:

$$\rho\frac{\partial v}{\partial t} = -\frac{\partial p}{\partial x} + \frac{\partial \tau_{yx}}{\partial x} \tag{2.14}$$

This equation can be represented on macroscopic basis by integrating over the control volume. As stated in [10], integration gives

$$\frac{d\bar{v}}{dt} = \frac{1}{m}(-A_p\Delta p + A_s\tau_w) \tag{2.15}$$

where A_s is the inside surface area of the conduit, $\bar{v}$ is the bulk flow velocity, and τ_w is the wall shear stress. The wall shear stress can be found from friction calculations, described in section 3.2.2. The term $A_s\tau_w$ can also be expressed in terms of frictional pressure drop, $A_p\Delta p_f$. To obtain an equation for volumetric flow rate, bulk flow velocity can be multiplied with the cross-sectional area of the conduit, giving

$$\frac{dQ}{dt} = \frac{1}{m}(-A_p\Delta p + A_p\Delta p_f). \tag{2.16}$$

If other losses are present in the flow, such as bends and valves, these can also be expressed in terms of Δp and simply added to the equation.

2.3.3 Conservation of Energy

The first law of thermodynamics states that energy is a conserved quantity, ie. energy cannot vanish, only be transformed from one form to another. For a closed system, i.e. no mass transfer across boundaries, the total energy will be constant, and can be expressed by the formula

$$\Delta U = Q - W \tag{2.17}$$

Here, ΔU is the change in internal energy of the system, Q is the heat supplied *to* the system, and W is the work done *by* the system *on* its surroundings.

If mass transfer is permitted across the boundaries, the system is referred to as an open system. When mass is flowing into the system it will perform work *on* the system in terms of *flow work*. This can be viewed as the work done on the system as the flow is "pushed" in or out of the system. It can be shown that the mathematical expression for flow work is:

$$W_{flow} = pV \tag{2.18}$$

The flow will also contain internal energy that will be provided to the system. Since the combined flow work and internal energy of a flow often occurs in thermodynamic calculations, a thermodynamic property called *enthalpy* is defined. This property is defined only for the sake of simplicity and convenience, and is not a physical property in itself. Enthalpy is often written as H, and the mathematical formula is given as

$$H = U + pV \tag{2.19}$$

From equation 2.17, an energy balance on differential form can be set up for an open control volume with mass entering and leaving the volume:

$$\frac{dU}{dt} = Q - W + H_{in} - H_{out} \tag{2.20}$$

Where H_{in} and H_{out} are the enthalpies entering and leaving the volume, and are defined as

$$\begin{aligned} H_{in} &= \dot{m}_{in} h_{in} \\ H_{out} &= \dot{m}_{out} h_{out} \end{aligned} \tag{2.21}$$

with the lower case h being the specific enthalpy, $h = \frac{H}{m}$.

In thermodynamics it is common to set up the energy balance in terms of enthalpy [11]. Introducing $U = H - pV$ gives the energy balance on the form

$$\frac{dH}{dt} = H_{in} - H_{out} + Q - W + p\frac{dV}{dt} + V\frac{dp}{dt} \tag{2.22}$$

$\frac{dH}{dt}$ can also be expressed as $\frac{dH}{dt} = m\frac{dh}{dt} + h\frac{dm}{dt}$. With $\frac{dm}{dt}$ being the mass balance, the energy balance can be set up on mass flow basis as

$$m\frac{dh}{dt} = \dot{m}_{in}(h_{in} - h_{cv}) - \dot{m}_{out}(h_{out} - h_{cv}) + Q - W + pdV + Vdp \tag{2.23}$$

As the equation of state for pressure uses temperature, it is desirable to express the energy balance in terms of temperature. This requires some more algebraic manipulation. First, as the pressure is a function of temperature,

an expression of its derivative is needed. In this thesis, the Redlich-Kwong equation of state will be used, and therefore, this is used when deriving the energy balance. The Redlich-Kwong equation is defined as

$$p = \frac{R_m T}{V_m - b} - \frac{a}{\sqrt{T} V_m (V_m + b)}. \tag{2.24}$$

with a and b being constants dependent on critical temperature and pressure and R_m being the specific gas constant.
The time dependent variables in this expression is T and V_m, giving the time derivative of pressure as

$$\frac{dp}{dt} = \left(\frac{\partial p}{\partial T}\right)\frac{dT}{dt} + \left(\frac{\partial p}{\partial V_m}\right)\frac{dV_m}{dt}. \tag{2.25}$$

For ideal gas, the enthalpy is only dependent on temperature, and defined as

$$h = \int_{T_{ref}}^{T} c_p dT. \tag{2.26}$$

where T_{ref} is the temperature at a chosen reference state, and c_p is the specific heat at constant pressure. The change in specific heat is often regarded constant, and can be taken outside the integral.
As stated, this only applies to ideal gases. As the Redlich-Kwong equation represents a non-ideal gas, the enthalpy will also be dependent on pressure. The "real" enthalpy can be calculated using residual properties. The residual property gives the enthalpy as a deviation from the ideal enthalpy:

$$h = h_{id} + h_{res} \tag{2.27}$$

where the subscripts "id" and "res" refers to ideal and residual properties, respectively.
It can be shown that for the Redlich-Kwong equation, the residual enthalpy term will be

$$h_{res} = \frac{bR_m T}{V_m - b} - \frac{a}{\sqrt{T} V_m + b} - \frac{3a}{2\sqrt{T} b} ln\left(\frac{V_m + b}{V_m}\right) \tag{2.28}$$

The $\frac{dh}{dt}$ term on the left hand side in equation 2.23 is the time derivative of the combined ideal and residual enthalpy. Derivation of these two requires the partial differential of h in regards to T and V_m:

$$\frac{dh}{dt} = \left(\frac{\partial h}{\partial T}\right)\frac{dT}{dt} + \left(\frac{\partial h}{\partial V_m}\right)\frac{dV_m}{dt}. \tag{2.29}$$

Omitting the details, it can be shown that the energy balance in terms of temperature will look like

$$\frac{dT}{dt} = \frac{H_{in} - H_{out} - h\frac{dm}{dt} + Q - W + \left(\frac{V}{m_{cv}}\left(\frac{\partial p}{\partial V_m}\right) + m_{cv}\sigma(t)\right)\frac{dV_m}{dt}}{m_{cv}\left(c_p + \frac{bR}{V_m - b} + \frac{a}{2T^{\frac{3}{2}}(V_m+b)} + \frac{3a}{4T^{\frac{3}{2}}b}\ln\frac{V_m+b}{V_m}\right) - V\frac{\partial p}{dT}} \tag{2.30}$$

with
$\sigma = \frac{bRT}{(V_m-b)^2} + \frac{a}{\sqrt{T}(V_m+b)^2} + \frac{3a}{2\sqrt{T}V_m(V_m+b)}$.

Chapter 3

Method

3.1 Overview

As mentioned in previous chapters, the CMC system is a hydro-pneumatic driven system. In regards to modelling, it will be natural to divide the system into two parts: the hydraulic side and the gas side. The computational method and governing equations are essentially similar to each other, but there are some material properties that has to be treated with care. While hydraulic oil is relatively stiff, gas is highly compressible. Therefore, density is an important aspect when modelling gas behaviour, and is computed explicitly. Together with volumetric flow and temperature, this is combined in a suitable equation of state. In some cases the hydraulic side will be isolated from the pneumatic system via the isolation valve. In this configuration the compressibility of the hydraulic liquid will be important due to high forces, and cannot be neglected. Depicted in figure 3.1 is a simplified conceptual drawing of the CMC system, with the hydraulic side marked with green and the gas side marked with blue.

3.2 Hydraulics

For modelling purposes, the main components of the hydraulic system is the plunger cylinder, isolation valve, hydraulic piping and the force equalizer cylinders. Compared to gas, the temperature variation in liquids will be of less importance. Therefore, the temperature is assumed constant in the modelling of hydraulics.
When performing dynamic simulations of hydraulic systems, compressibility of hydraulic liquid will be important to accurately simulate the real behaviour of the system [12]. The compressibility of liquid is described by the bulk modulus, β, and will affect the pressure gradient. Therefore, the density is assumed constant, and not expressed explicitly in the hydraulic computations. Compressibility will be accounted for in a differential equa-

tion for the pressure gradient via the bulk modulus.
The system is viewed as a "flow circulation system", meaning that positive flow will be defined going *from* the plunger cylinder, *to* the accumulator, consequently. This is shown in figure 3.2, where the flow is shown in positive direction. Figure 3.2 also shows numbering for each segment used in this text.

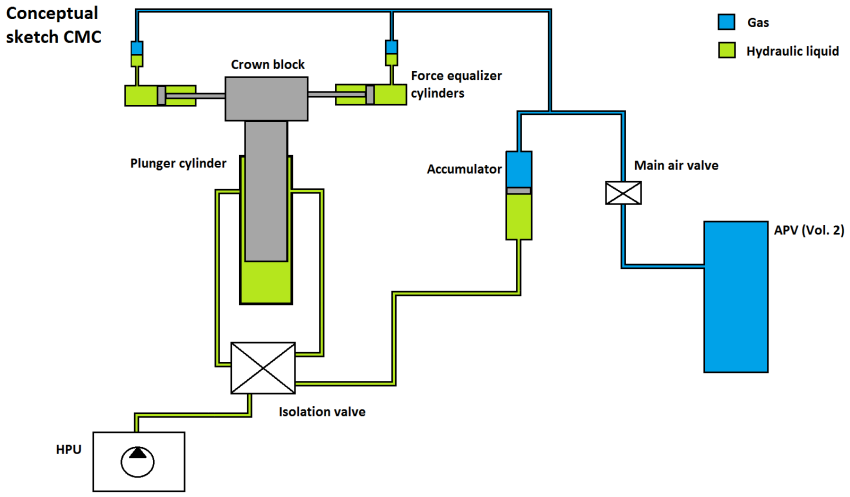

Figure 3.1: Conceptual drawing of CMC system

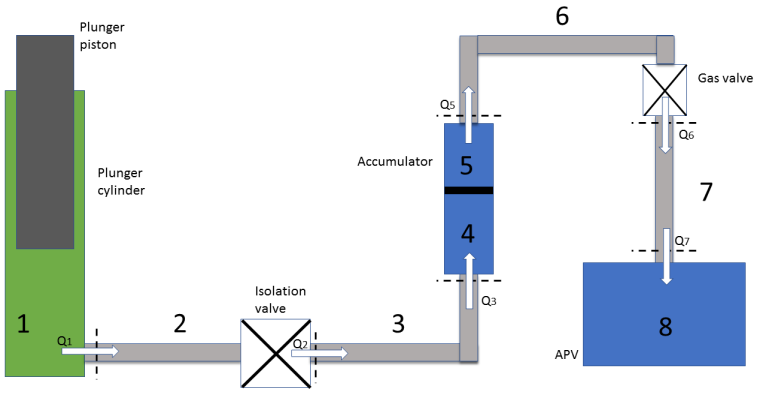

Figure 3.2: Simplified drawing of the CMC system, with positive defined flow and numbering of segments

3.2.1 Plunger Cylinder

The plunger cylinder is a single-acting cylinder with one chamber housing a plunger piston. To fully describe the cylinder dynamics, two state variables are needed: piston velocity, v_{piston}, and piston position, y_{piston}. From these two variables, pressure, flow and volume can be calculated, which will affect the rest of the system system.
In the model, two different reference frames are introduced. This gives two different notation for velocity and position: v_{abs}, y_{abs} and v_{rel}, y_{rel}. The subscript "abs" refers to absolute velocity and position of the plunger piston, and is measured with respect to the sea bed. The aim of the compensation system is to keep variation of the absolute piston movement to a minimum. As this is a passive system it will not be able to compensate perfect and some movement is expected.
To keep the variation of the absolute piston position as small as possible, the piston, relative to the cylinder, has to counteract the rig heave motion. This motion is referred to as the relative piston position, with the subscript "rel". The relative motion is defined as

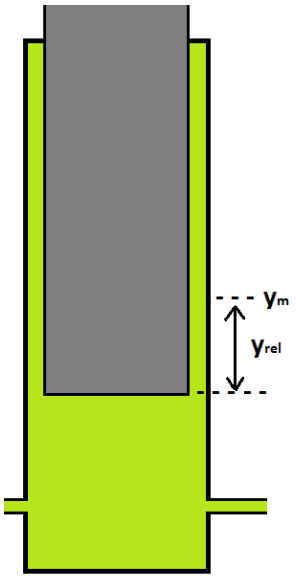

Figure 3.3: Plunger cylinder with frame of referance

$$\begin{aligned} v_{rel} &= v_{abs} - v_{rig} \\ y_{rel} &= y_{abs} - y_{rig} \end{aligned} \tag{3.1}$$

where v_{rig} and y_{rig} refers to the rig heave velocity and position, respectively. The reference frame of the relative motion is chosen to be in the middle of the cylinder, y_m, and can be seen in figure 3.3.

To express the piston velocity and position, its first-order time derivatives are needed. The time derivative of v_{piston} is the piston acceleration and can be expressed via Newtons 2nd law:

$$\frac{dv_{piston}}{dt} = \frac{\sum F}{m_{piston}} \tag{3.2}$$

where $\sum F$ is the sum of forces acting on the piston, and m_{piston} is the piston mass. Figure 3.4 shows a simplified sketch of the forces acting on the piston in a typical drilling situation.
Depending on the operation, there are several forces acting on the piston. The plunger cylinder is connected to the crown block, which holds the weight

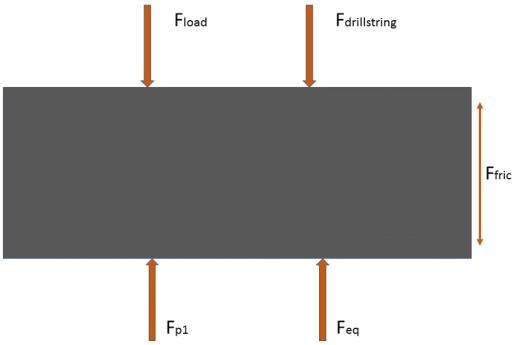

Figure 3.4: Forces acting on the plunger piston

from the drilling equipment. The weight of the equipment will exert a negative (downwards) force, on the piston. The weight of the piston will also contribute to a negative force. For the sake of simplicity, these two forces can be combined to a total downwards force referred to as F_{load}.

While drilling, there will be more complex forces acting on the piston. There will be friction between the well and the drill string, friction due to circulating fluid and force variation due to the elasticity in the drill string and wires. It is beyond the scope of this thesis to investigate these effects. To compare results between the model and available log data, these effects are accounted for by assuming that the force variation that occurs will act as a spring-damper system, where spring coefficients and damping coefficients are tuned manually. This leads to the simple expression

$$F_{drillstring} = k_{eq} \cdot y_{abs} + c_{eq} \cdot v_{abs} \tag{3.3}$$

where k_{eq} is the equivalent spring coefficient for all these effects and c_{eq} is the equivalent damping factor.
Note: This is a very simplified approach, and only used for obtaining a piston movement to go with the logged data for verifying pressure and flow results in the CMC model. To obtain a more realistic results one should look into the mentioned effects in more detail.

The hydraulic pressure in the cylinder, p_1, is acting on the piston, causing a force in positive (upward) direction. This force is counteracting the forces acting downwards and is given by

$$F_{p1} = p_1 A_{piston} \tag{3.4}$$

with A_{piston} being the cross sectional piston area.

Also, as the plunger is moving through the hydraulic fluid in the cylinder, it will cause friction between the fluid and piston. The friction will act as a damper on the piston movement, and is modelled as a linear damper with the expression

$$F_{fric} = -sign(v)\ c_{piston}\ v_{rel} \tag{3.5}$$

where c_{piston} is the damping coefficient. Friction will always act in opposite direction of the movement, thus the sign function in equation 3.5.

Lastly, the force from the equalizer cylinders is computed. These cylinders are driven by the pressure in the pneumatic system and are contributing to less load variation by exerting a force counteracting the forces from the heave motion. These cylinders can be seen overlaying the crown block in figure 3.1. To keep a modest level of complexity in the model, these cylinders are not modelled explicitly. Instead, the gas pipes are added as extra volume in the pneumatic system, and the force exerted on the crown block are obtained from empirical table values. In total, this leads to the force F_{eq} acting on the the piston. For a positive piston displacement, the force equalizers are exerting a positive force on the piston, and vice versa.
Replacing $\sum F$ in equation 3.2 with the above forces, and noting that the time derivative $\frac{dy_{rel}}{dt}$ is simply the same as the relative velocity, gives the relations

$$\frac{dv_{piston}}{dt} = \frac{F_{p1} + F_{eq} - F_{fric} - F_{load} - F_{drillstring}}{m_{piston}} \tag{3.6}$$

$$\frac{dy_{rel}}{dt} = v_{piston} \tag{3.7}$$

which will be used to calculate the new states of the piston velocity and position.

To obtain the pressure in the cylinder, the pressure gradient has to be calculated. With the assumption of constant density, the equation for the rate of change in pressure is given as [12]:

$$\frac{dp_1}{dt} = \frac{\beta}{V_1}\left(Q_1 - \frac{dV_1}{dt}\right) \tag{3.8}$$

with β being the bulk modulus.

The time rate of change in volume for the plunger cylinder is dependent on the relative velocity of the piston. Thus, the volume is given by the differential equation

$$\frac{dV_1}{dt} = A_{piston} \cdot v_{rel} \tag{3.9}$$

For this model, the return line is neglected and it is assumed that there is just one pipe in the cylinder. Therefore, in the plunger cylinder there is just one flow in and out of the volume, namely Q_1. The differential equation for flow rate earlier conducted in section 2.3.2, is based on the acceleration of a certain amount of fluid. It would be difficult to find an expression which takes into account how much of the fluid that actually would enter the pipe, since most of the fluid would remain in the cylinder. Therefore, an empirical based orifice equation based on the pressure difference and density will be used to calculate the flow directly. This will be an approximation of the flow entering and leaving the cylinder, without having to set up a differential equation for the flow rate. The orifice equation is given as [12]:

$$Q_1 = C_D A_{hyd} \sqrt{\frac{2}{\rho_{oil}} \Delta p_{dyn}(t)} \tag{3.10}$$

where
C_D = Discharge coefficient
A_{hyd} = Cross sectional area of hydraulic pipe
ρ_{oil} = Oil density
$\Delta p_{dyn} = p_1(t) - p_2(t)$

The flow is entering the hydraulic pipe, therefore it is important to note that the cross sectional area used in equation 3.10 is for the hydraulic pipe. As stated earlier, the positive flow direction is *from* the plunger cylinder *to* the accumulator. Thus, when Q_1 is positive, the flow is leaving the plunger cylinder

3.2.2 Hydraulic piping

The hydraulic pipes are connecting the plunger cylinder to the accumulator via the isolation valve. The isolation valve controls the flow between the cylinder and accumulator, but can also isolate the cylinder if desired. In the piping there are no moving parts, only fluid flow. The two defining states for the piping are the flow Q_n, and pressure p_n, where the subscript "n" denotes numbering of the component. In this text, "n" for the hydraulic piping will be pipe segment 2 or 3, as seen in figure 3.2
The pipes will always have one flow entering its control volume, Q_{in}, and one flow leaving the control volume, Q_{out}. A cross section of he piping is shown in figure 3.5.
The flow into the control volume is the flow out of the former component, and is therefore already known. The flow out of the control volume has to

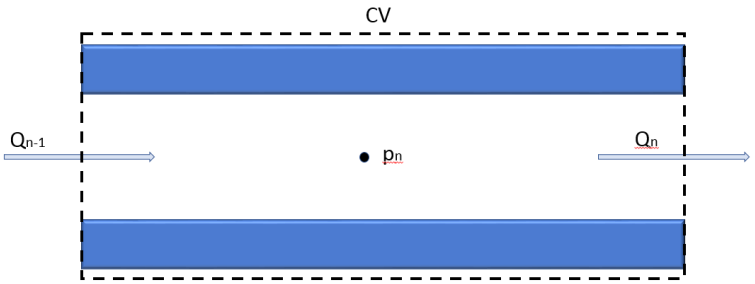

Figure 3.5: Cross section of piping

be computed, and the expression for flow rate deduced in section 2.3.2 is used. This gives the flow rate out of the control volume as

$$\frac{dQ_n}{dt} = \frac{A_{hyd}^2}{m_n}(-\Delta p_{dyn} + \Delta p_{valve} + \Delta p_{bend} + \Delta p_{fric}) \tag{3.11}$$

where
m_n = Mass present in component n
$\Delta p_{dyn} = p_{n-1} - p_n$
Δp_{valve} = Pressure drop over valve
Δp_{bend} = Pressure drop over bends
A_{hyd} = Cross sectional area of hydraulic pipes
A_s = Inside surface area of pipe
τ_w = Wall shear stress

Flow in pipes will always experience friction along the pipe wall [13]. This leads to loss of energy able to perform work and results in a pressure loss in the direction of the flow. The relation between pressure loss and flow rate can be described by the *Darcy-Weisbach equation* [14]. This equation is expressed in terms of head loss and is given as

$$h_L = f\frac{L}{D}\frac{v^2}{2g} \tag{3.12}$$

with
h_L = Head loss
f = Friction factor to be determined
L = Length of conduit
D = Diameter of conduit
v = average flow velocity
g = gravitational acceleration

To use the Darcy-Weisbach equation in the presented flow rate equation, it should be expressed in terms of pressure drop, Δp. It can be shown [13]

that

$$\Delta p = h_L \rho g \tag{3.13}$$

where g is the gravitational acceleration term. The Darcy-Weisbach equation on pressure drop form can then be expressed as

$$\Delta p_{fric} = \frac{\rho f_D L v_n^2}{2D} \tag{3.14}$$

with f_d being the Darcy friction factor. The velocity will be given by $v = \frac{Q_n}{A_{hyd}}$.

Traditionally, the determination of the Darcy friction factor is computed iteratively [15], and therefore it has been conducted a lot of research based on empirical data to find approximated formulas. As expected, there is a difference in the behaviour of the friction factor depending on the flow patterns. Findings show that for laminar flow ($Re < 2000$) the friction factor is only dependent on Reynolds number, Re, and can be given by the formula

$$f_D = \frac{64}{Re} \tag{3.15}$$

For turbulent flow ($Re > 4000$) however, roughness of the pipe wall has to be taken into consideration. One of the most recognized formulas for finding the friction factor is the *Colebrook-White equation* [13]. This equation expresses the Dracy friction factor as a function of Reynolds number and relative pipe roughness, $\frac{\epsilon}{D}$, and is fitted to experimental studies of turbulent flow in smooth and rough conduits. This equation is used to iteratively solve for the friction factor. Iterative methods requires more computations to be carried out than for direct solutions, and therefore, approximated direct solutions has been proposed over the years. The model for the CMC system presented in this thesis is solved by euler integration, and it would not be favourable to include iterative procedures to find the friction factor. A alternative to the Colebrook-White equation has been proposed by Professor S.E. Haaland [16]. This equation computes the friction factor directly for a full-flowing circular pipe, and has been proved to be well within the accuracy of experimental data. The equation is given as

$$\frac{1}{\sqrt{f_D}} = -1.8 log_{10} \left[\left(\frac{\frac{\epsilon}{D}}{3.7} \right)^{\frac{10}{9}} + \frac{6.9}{Re} \right] \tag{3.16}$$

It is hard to find exact values for the relative pipe roughness, as this will vary with wear and tear. Values are usually found from empirical data listed in tables. Since the equations for the friction factor is already based on approximation of empirical data it is assumed that the error from pipe roughness value will have relatively small effects.

As can be seen in figure 3.1, there is an isolation valve within the hydraulic piping. For modelling purposes, the valve will act like a flow restriction, and modelled thereafter. Different types of valves will have different characteristics, depending on function, shape, manufacturer etc. To keep flexibility regarding choice of valves a standard orifice equation is chosen to represent the valve. The general flow equation for an orifice is given as

$$Q = C_d A_0 \sqrt{\frac{2}{\rho} \Delta p_{valve}} \tag{3.17}$$

with Q being volumetric flow, and A_0 being the cross sectional area at the entrance of the orifice.
The pressure loss over the valve will affect the flow through the pipe. To add this pressure loss to the flow rate equation (equation 3.11), equation 3.17 is rearranged in terms of Δp_{valve}:

$$\Delta p_{valve} = \frac{\rho}{2(C_D A_{hyd})^2} Q_n^2 \tag{3.18}$$

The term Δp_{bend} encountered in equation 3.11 is the pressure loss due to bends. There are several sources leading to the pressure drop over a bend. Conventionally, the head loss is assumed to consist of loss due to curvature, excess loss in the downstream tangent and loss due to the length of the bend [13]. The pressure drop is computed in accordance with the head loss in the Darcy-Weisbach equation. A new constant K_b is introduced, which is known as the *bend coefficient*. This coefficient is an empirical constant which takes the mentioned sources of head loss into account for easy computation. The bend coefficient is analogous to $f\frac{L}{D}$ in the computation of friction, and gives the head loss for bends as

$$h_b = K_b \frac{v_n^2}{2g} \tag{3.19}$$

In the Darcy-Weisbach equation, pressure drop can be expressed via head loss as $\Delta p = h_L \cdot \rho \cdot g$, giving the pressure drop of bends as:

$$\Delta p_{bends} = K_b \, \frac{\rho v_n^2}{2} \tag{3.20}$$

As there are no moving parts in the piping, the pressure will be defined by flow into and out of the pipe segment. The rate of change in pressure will thus be

$$\frac{dp_n}{dt} = \frac{\beta}{V_n} \cdot (Q_{n-1} - Q_n) \tag{3.21}$$

3.2.3 Accumulator (hydraulic side)

The accumulator is divided into two sides: the hydraulic side and the gas side. The two sides are divided by a piston, and the hydraulic fluid will flow into the accumulator, exerting a pressure force from underneath the piston. The accumulator is shown in figure 3.6. As for the plunger cylinder, there is a moving piston, which needs two state variables to fully describe its dynamics. The piston divides the accumulator into two chambers, and it is assumed that leakage between the chambers can be neglected. The piston is not connected to any external equipment, and the inertial forces from the rig movement is neglected. Thus, there is only one frame of reference that need to be taken into consideration. As shown in figure 3.6, this reference frame, y_m is placed in the middle of the accumulator, as also done for the plunger cylinder. The state variables for the accumulator piston is the velocity, v_{acc}, and the position, y_{acc}.
Following the same numbering as in figure 3.2, there are two pressure forces acting on the accumulator piston: pressure force from the hydraulic side, referred to as F_{p_4}, and pressure force from the gas side, referred to as F_{p_5}. The forces are calculated as

$$F_{p_4} = p_4 A_4 \tag{3.22}$$
$$F_{p_5} = p_5 A_4 \tag{3.23}$$

where A_4 is the cross sectional area of the accumulator.

There will also be the weight of the piston, F_{acc}, and a friction force acting along the side of the piston against the accumulator wall, F_{f_2}.
Summing these forces and utilizing Newtons 2nd law, the acceleration of the piston will be

$$\frac{dv_{acc}}{dt} = \frac{F_{p_4} - F_{p_5} - Facc - F_{fric}}{m_{acc}} \tag{3.24}$$

with m_{acc} being the piston mass.
As for the plunger cylinder, the first derivative of position equals velocity of the piston:

$$\frac{dy_{acc}}{dt} = v_{acc} \tag{3.25}$$

To calculate the pressure in the hydraulic side of the accumulator, the rate of change in pressure has to be computed. Following in the same manners as for the plunger cylinder, this gives:

$$\frac{dp_4}{dt} = \frac{\beta}{V_4}\left(Q_4 - \frac{dV_4}{dt}\right) \tag{3.26}$$

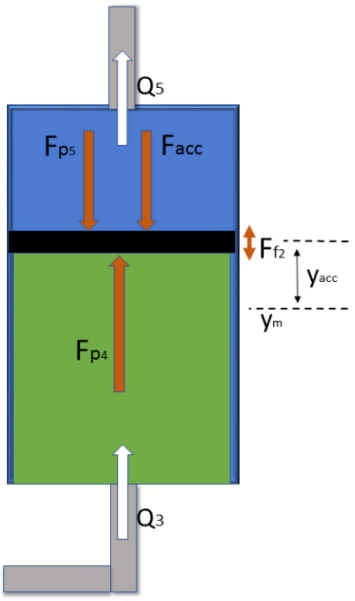

Figure 3.6: Accumulator with forces on piston. Also the flows Q_3 and Q_5 are shown in positive direction

The rate of change in volume will also be carried out as in the plunger cylinder, giving

$$\frac{dV_4}{dt} = A_4 \cdot v_{acc} \tag{3.27}$$

There is one hydraulic pipe connected to the accumulator. As the fluid entering the accumulator will be the same as the fluid leaving the last pipe segment, the realtion

$$Q_4 = Q_3 \tag{3.28}$$

can be set up. The sign of Q_3 will decide if the flow is entering or leaving the accumulator.

3.3 Pneumaitcs

The pneumatic system consists of the gas side of the accumulator, piping, air valve and air pressure vessels (APV's). To avoid adding more complexity to the model, the force equalizer cylinders that can be seen in figure 3.1 are neglected for the following calculations. Instead of modelling these cylinders explicitly, some extra volume is added to the gas piping. The forces from the force equalizer cylinders are obtained from empirical table values, and

are accounted for in the force balance for the plunger piston. The flow to the force equalizer cylinders will affect the total system, but it is assumed that this effect will be relatively small compared to the flow between the accumulator and APV's.
The high compressibility of gas calls for a slightly different approach in regards to modelling. For hydraulics, density could be regarded as approximately constant, and the bulk modulus accounted for the compressibility in the pressure equation. For gas however, the density will be far more important and appear as a state variable in itself. Density of gases is much more sensitive to temperature than liquids [17]. Therefore, the temperature will also be of more importance for gas behaviour. Density, together with volumetric flow and temperature, will be related through an Equation of State (EOS) to fully describe the gas behaviour.
As done for the hydraulics, the system is viewed as a "flow circulation system". This defines positive as going *from* the accumulator, *to* the APVs, as shown in figure 3.2.

3.3.1 Accumulator (gas side)

The gas side of the accumulator function in the same manner as the hydraulic side. There is one flow in or out of the accumulator, depending on the direction of the flow. The flow *out* of the accumulator is based on a static orifice equation, as justified in section 3.2.1. The piston motion is already described in section 3.2.3, and will be common for the volume calculations on both sides.
The rate of change of volume is given by the equation

$$\frac{dV_5}{dt} = -A_5 \cdot v_{acc}. \tag{3.29}$$

As can be seen in figure 3.6, a positive displacement of the accumulator piston yields a negative change in volume for the gas side, and thus the minus sign in equation 3.29.

As previously stated, for the pneumatic calculations, density will appear as a state variable and is calculated explicitly. Based on the theory in section 2.3.1, the equation for rate of change in density is given as

$$\frac{d\rho}{dt} = \left(\rho_{in}Q_{in} - \rho_{out}Q_{out} - \rho\frac{dV}{dt}\right) \tag{3.30}$$

As there is only one pipe connected to the accumulator, there cannot be flow in and out of the accumulator at the same time. The flow terms will therefore be replaced by only one flow term, Q_5, giving the flow rate as

$$\frac{d\rho_5}{dt} = \left(\rho_5 Q_5 - \rho_5\frac{dV_5}{dt}\right) \tag{3.31}$$

Mass, m, at each time instant is calculated from rearrangement of the definition of density, giving

$$m_5 = \rho_5 V_5 \tag{3.32}$$

The chosen equation of state in this thesis is the Redlich-Kwong equation, and it is common to state this equation in terms of specific volume instead of density. Specific volume is defined as

$$V_{m_5} = \frac{m_5}{V_5} = \frac{1}{\rho_5}. \tag{3.33}$$

As described in section 2.3.3, the temperature equation will be dependent of pressure. As can be seen in equation 2.30, this requires an expression for the time derivative of specific volume. From the definition of specific volume this gives

$$\frac{dV_{m_5}}{dt} = \frac{-1}{\rho_5^2}\frac{d\rho_5}{dt} \tag{3.34}$$

As stated in the introduction of this section, the flow leaving the accumulator is given by the equation

$$Q_5 = C_D A_{gas}\sqrt{\frac{2}{\rho_5}\Delta p_{dyn}} \tag{3.35}$$

where A_{gas} is the cross sectional area of the gas pipes, and $\Delta p_{dyn} = (p_5 - p_6)$. As for the plunger cylinder and the hydraulic side of the accumulator, the flow rate equation from section 2.3.2 will be used to calculate flow *into* the accumulator from the gas pipes.

As stated in section 3.3, temperature will be more important for gas modelling then for hydraulics due to the fact that density of gas is more sensitive to temperature variation than liquids [17]. Thermodynamic analysis for compressible fluid, especially when the fluid is not considered ideal, quickly ends up with relatively complex expressions. In this section the temperature equation is given without an explanation, and the reader is referred to section 2.3.3 where the the temperature model is thoroughly treated.

When the gas flow enters a new volume, perfect mixing is assumed. This means that the temperature, density and pressure will be uniformly distributed across the volume, and the gas *leaving* the volume will be in the

same state as the the rest of the volume. From equation 2.30, one can see that the second term on the right hand side will vanish as $h_{out} = h_{cv}$ with this assumption. Hence, the outflow term will vanish, while the inflow term will remain. The term h_{in} for a volume, will always be equal to h_{cv} for the volume the flow is coming from.
Given these assumptions and observations, the rate of temperature change will be:

$$\frac{dT}{dt} = \frac{\dot{m}_{in}(h_{in} - h_{cv}) + Q - W + \left(\frac{V}{m_{cv}}\left(\frac{\partial p}{\partial V_m}\right) + m_{cv}\sigma(t)\right)\frac{dV_m}{dt}}{m_{cv}\left(c_p + \frac{bR}{V_m - b} + \frac{a}{2T^{\frac{3}{2}}(V_m+b)} + \frac{3a}{4T^{\frac{3}{2}}b}\ln\frac{V_m+b}{V_m}\right) - V\frac{\partial p}{dT}}. \tag{3.36}$$

Note that the term $\sigma(t)$ is introduced. This is a definition made only to simplify the expression, and is not a physical quantity. $\sigma(t)$ is given as: $\sigma(t) = \frac{bRT}{(V_m-b)^2} + \frac{a}{\sqrt{T}(V_m+b)^2} + \frac{3a}{2\sqrt{T}V_m(V_m+b)}$.

To obtain the gas pressure, it is common to use an equation of state (EOS). An equation of state is a semi-empirical thermodynamic equation describing the state of matter under a given set of physical conditions [18] [3]. As stated in previous chapters, there are a lot of different EOS' for gas behaviour. The Redlich-Kwong equation is an equation widely used for engineering calculations [19], and is chosen for the calculation of gas pressure in this thesis. The pressure in the accumulator is calculated as

$$p_5 = \frac{RT_5}{V_{m5} - b} - \frac{a}{\sqrt{T_5}V_m(V_m + b)}. \tag{3.37}$$

where

$$a = 0.42748\frac{R^2T_c^{2.5}}{p_c} \tag{3.38}$$

$$b = 0.08664\frac{RT_c}{p_c} \tag{3.39}$$

with R being the specific gas constant. T_c and p_c are the critical temperature and critical pressure, respectively.

3.3.2 Gas piping

The gas pipes are connecting the accumulator to the Air Pressure Vessels (APVs). The air valve is controlling the amount of flow to the APVs, and thus regulates the stiffness of the gas system. Less flow means higher pressure in the accumulator, which results in a quicker response to piston movement in the accumulator. As for the hydraulic piping, pressure and flow are

two defining states but also the temperature is regarded as a state variable in the pneumatic modelling. Graphically, the gas piping will be similar to the hydraulic piping, and the reader is referred to figure 3.5 for a graphical representation.
For the gas piping, in accordance with figure 3.2, the subscript "n" refers to pipe segment 6 or 7.

The general expression for rate of change of density is given in equation 3.30. As there are no moving parts in the piping, the last term in equation 3.30 vanishes. Hence, the density gradient is only dependent on the amount of mass entering and leaving the control volume:

$$\frac{d\rho_n}{dt} = (\rho_{n-1}Q_{n-1} - \rho_n Q_n)\,. \tag{3.40}$$

As the density is known, mass can easily be calculated by,

$$m_n = \rho_n V_n \tag{3.41}$$

The flow rate equation used in section 3.2.2 yields for compressible fluid in general. Therefore, the equation will also be applicable for gas flow. The equation for the flow rate in the gas pipe will look like,

$$\frac{dQ_n}{dt} = \frac{A_{gas}^2}{m_n}(-\Delta p_{dyn} + \Delta p_{valve} + \Delta p_{bends} + \Delta p_{fric}) \tag{3.42}$$

with A_{gas} being the cross sectional area of the gas pipes.

The Darcy friction factor is also applicable for gas flow, and will be applied in the same manner as for the hydraulic piping. As gas is considerably less dense than liquid, and thus less viscous, the shear stress at the wall will be much less than for liquid. Therefore, the frictional pressure drop will be considerably less for gas flows. For convenience, the equations for calculating the friction constant and pressure drop is repeated:

$$f_D = \frac{64}{Re} \quad (laminar\ flow) \tag{3.43}$$

$$\frac{1}{\sqrt{f_D}} = -1.8log_{10}\left[\left(\frac{\frac{\epsilon}{D}}{3.7}\right)^{\frac{10}{9}} + \frac{6.9}{Re}\right] \quad (turbulent\ flow) \tag{3.16}$$

$$\Delta p_{fric} = \frac{\rho f_D L v_n^2}{2D} \tag{3.44}$$

As the gas has low viscosity compared to liquid, it is assumed that the surface wear of the inside of the gas pipes are less than for the hydraulic pipes.

Thus, a smaller relative roughness value will be chosen for the gas pipes.

To keep flexibility and simplicity in the model, the air valve is modelled in the same manner as the hydraulic valve. As described in more detail in section 3.2.2, the valve will act like a flow restriction, and appear as a pressure drop in the flow rate equation. The pressure drop will be described as in equation 3.18:

$$\Delta p_{valve} = \frac{\rho_n}{2(C_D A_{gas})^2} Q_n^2 \tag{3.45}$$

Pressure loss due to bends in the gas piping is calculated as in section 3.2.2. Using the Darcy-Weisbach equation in terms of pressure drop gives

$$\Delta p_{bends} = K_b \, \frac{\rho_n v_n^2}{2} \tag{3.46}$$

The temperature equation is almost similar to the temperature equation of the accumulator. The same assumption regarding perfect mixing is made, which eliminates the outflow. The difference is that there are no moving parts in the piping, hence, W is set to zero. For the piping, this gives:

$$\frac{dT}{dt} = \frac{\dot{m}_{in}(h_{in} - h_{cv}) + Q + \left(\frac{V}{m_{cv}}\left(\frac{\partial p}{\partial V_m}\right) + m_{cv}\sigma(t)\right)\frac{dV_m}{dt}}{m_{cv}\left(c_p + \frac{bR}{V_m - b} + \frac{a}{2T^{\frac{3}{2}}(V_m + b)} + \frac{3a}{4T^{\frac{3}{2}}b}\ln\frac{V_m + b}{V_m}\right) - V\frac{\partial p}{dT}}. \tag{3.47}$$

The Redlich-Kwong equation is used for expressing the pressure directly in each volume. For the gas piping this gives

$$p_n = \frac{RT_n}{V_{m,n} - b} - \frac{a}{\sqrt{T_n}V_{m,n}(V_{m,n} + b)}. \tag{3.48}$$

3.3.3 Air Pressure Vessel (APV)

APVs are divided into two groups: working APVs and standby APVs. The working APVs provide an auxiliary volume for the gas to enter. The APVs consists of several connected gas bottles, making it possible to vary the volume if desired. In this model it is assumed that the volume is set at the beginning of operation, leading to a constant volume for the APVs. The aim is to obtain a low weight on bit variation, which calls for a flexible

gas spring. This is achieved by having a large auxiliary volume for the gas to flow into. The working APVs can provide up to seven times the initial volume of the accumulator. The standby APVs provide an air volume at higher pressure than the working APVs. This allows for an instant pressure increase by bleeding gas from the standby APVs to the working APVs if needed. This will change the stiffness of the system and can be viewed as the equivalent of increasing the spring stiffness coefficient for a conventional mechanical spring.

As can be seen in figure 3.1, there is only one pipe into the APVs. Hence, as described in earlier sections, the flow in and out of the APVs will be combined into one flow term, Q_8.

The volume is assumed constant while operating. Thus, there are no volume variations to account for in the density gradient, and the last term in equation 3.30 will vanish. Also, there are only one flow entering or leaving the volume, combined in Q_8. This leaves the expression for the density gradient looking like

$$\frac{d\rho_8}{dt} = \frac{1}{V_8}(\rho_8 Q_8) \tag{3.49}$$

The mass is calculated as before through the relation $m_n = \rho_n V_n$.

The temperature equation is set up for the APVs in the same manner as for the accumulator. There are no moving parts in the APVs and the volume is considered constant. As justified in section 3.3.2, the rate of change in temperature will be given as

$$\frac{dT}{dt} = \frac{\dot{m}_{in}(h_{in} - h_{cv}) + Q + \left(\frac{V}{m_{cv}}\left(\frac{\partial p}{\partial V_m}\right) + m_{cv}\sigma(t)\right)\frac{dV_m}{dt}}{m_{cv}\left(c_p + \frac{bR}{V_m - b} + \frac{a}{2T^{\frac{3}{2}}(V_m + b)} + \frac{3a}{4T^{\frac{3}{2}}b}\ln\frac{V_m + b}{V_m}\right) - V\frac{\partial p}{dT}}. \tag{3.50}$$

Lastly, the pressure in the APVs are calculated. Setting up the Redlich-Kwong equation gives:

$$p_8 = \frac{RT_8}{V_{m,8} - b} - \frac{a}{\sqrt{T_8}V_{m,8}(V_{m,8} + b)} \tag{3.51}$$

Chapter 4

Results and discussion

In this section, results from the simulations will be presented and discussed. First, the model will be compared to results from log data to verify the model performance. The log data is received from a logging unit on board a floating rig in drilling operation. When the model is verified it will be compared to simplified versions, where more ideal behaviour is assumed. This is done to identify differences between the ideal and non-ideal assumptions in the pressure and temperature region regarding this specific case. Also, a description of initial values and signal preparation for the model start-up is included.

4.1 Initial Values and Signal Preparation

To avoid large oscillations, and get a smooth start, reasonable initial values have to be set. The Redlich-Kwong equation is very sensitive to changes in density, and thus a good estimation of density at the start of the simulation is important. The initial pressure and temperature are set manually, where the pressure is found from log data. The log data contains no information about temperature, so the initial temperature is assumed to be 25 degrees Celsius. From these variables the density at the initial state can be found. For ideal gas yields the simple relation $\rho = \frac{p}{R_m T}$, but for the Redlich-Kwong EOS some more algebraic manipulation is necessary. It can be shown that solving the Redlich-Kwong EOS for specific volume ends up in a third degree polynomial:

$$V_m^3 - V_m^2 \left(\frac{R_m T}{p} \right) + V_m \left(\frac{a}{p\sqrt{T}} - b^2 - \frac{bR_m T}{p} \right) - \frac{ab}{p\sqrt{T}} = 0 \tag{4.1}$$

The specific volume is used to calculate the density via the relation $\rho = \frac{1}{V_m}$. From a mathematical perspective, equation 4.1 leads to three roots. For the model of the CMC system at hand, two of them are often imaginary, and it is clear which one will be the representative of the real density. In

case of three real roots, the most stable one should be used. One can also compare it to the ideal density, as the two will be in the vicinity of each other.

To validate the model, the results are compared to log data from an actual rig. The log data has a sampling rate of 50 Hz. The mathematical model might run with a sampling rate as high as 100 000 Hz to cope with the fast dynamics present in the system. The model uses the vertical rig motion from the motion reference unit (MRU) as input signal. As this signal comes at a rate of 50 Hz, the signal is converted to the desired sampling rate via linear interpolation between each sample. Due to discretization of a continuous motion in the MRU, and measurement noise, the signal contains a lot of sudden jumps. Therefore, the signal is filtered through a moving-average filter to obtain a smooth curve which is easier for Matlab to treat.

4.2 Log Data

The log data is received from a logging unit found on board a floating rig, and is recorded during a drilling operation. The drill string will be submerged into the well, causing the spring-damper force on the piston as explained in 3.2.1. The log data provides data for rig motion, plunger piston motion and pressures. The MRU (motion reference unit) logs the wave induced heave motion of the rig, and gives heave velocity and vertical heave position as two separate signals. The heave velocity is used as the input for the simulation model. The plunger piston velocity and position are logged, and are the same as relative piston position and velocity in section 3.2.1. There are placed pressure sensors in the plunger cylinder, APVs, and both sides of the accumulator. Log data from these sensors will be compared to the simulation model for verification of pressure.
Results from comparing simulation data for cylinder position to log data can be seen in figure 4.1.

Figure 4.1 shows that the relative cylinder position from the simulations follows the position obtained from log data without any excessive deviation. As the cylinder is the driver for the whole system, this is important in relation to further calculations. Note that the start of the calculated piston position is different from the log data. The simulation starts when the heave velocity is zero, which happens at 2.14 seconds. This is done to avoid excessive oscillations and spikes at the start of the simulation due to numerical issues that arises when the MRU velocity and cylinder acceleration does not match. The acceleration term could be calculated to fit with the MRU velocity, but for convenience, and less initial calculations, this is avoided when compared to the log data.

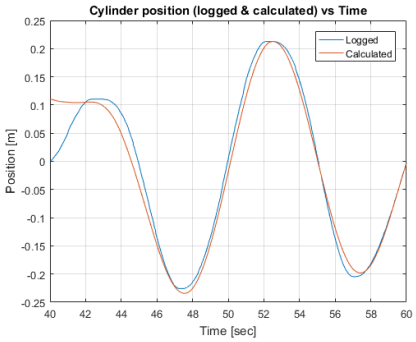

(a) Calculated relative cylinder position and logged relative cylinder position

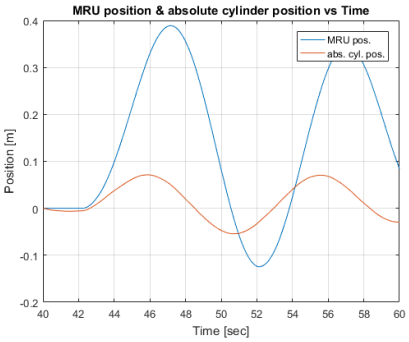

(b) Absolute cylinder position compared to MRU position. Shows degree of compensation for the system

Figure 4.1: Relative and absolute cylinder position

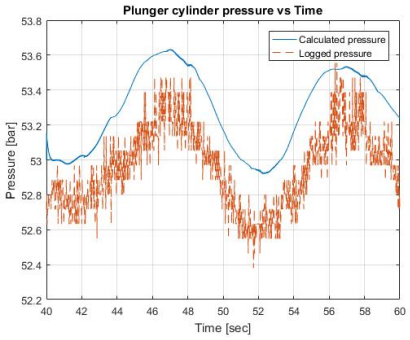

(a) Plunger pressure

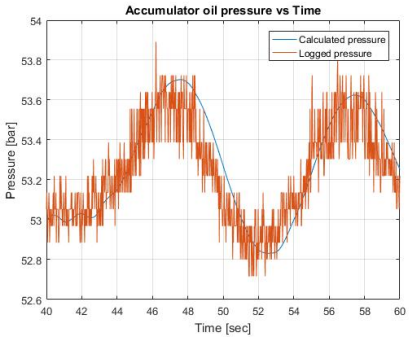

(b) Accumulator oil pressure

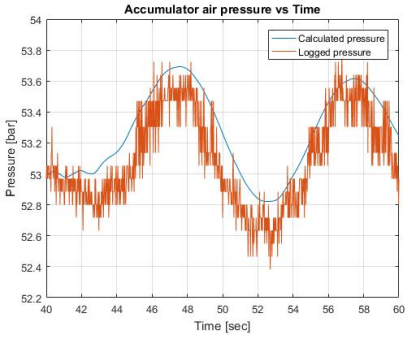

(c) Accumulator air pressure

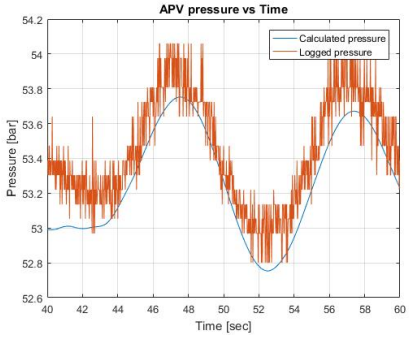

(d) APV pressure

Figure 4.2: Pressures CMC

The first results from comparing the simulated pressures to the logged pressures in the different volumes are illustrated in figure 4.2.

The recorded data is given from sensors placed on the rig, and there will always be measurement errors to some extent. Upon investigation of the log data, there seems like there might be an offset error between the pressure measurements. As can be seen in figure 4.3, the logged pressures behaves in a similar fashion, but is shifted in vertical direction.

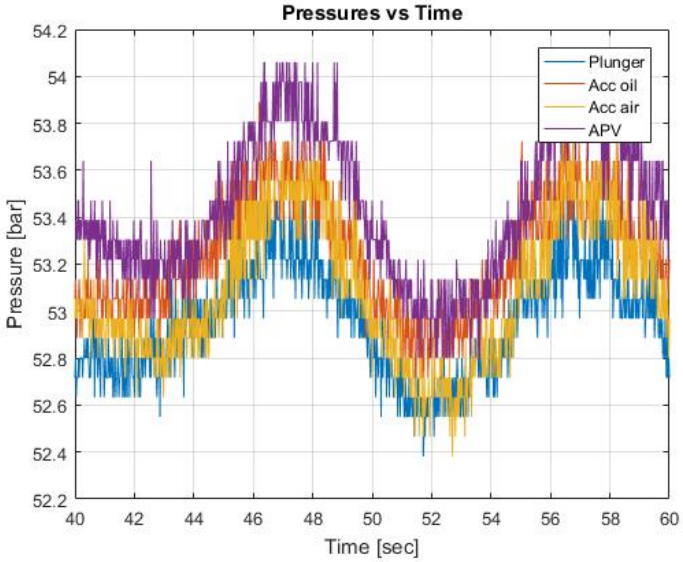

Figure 4.3: Logged pressures

It is expected that the pressure variation between the different volumes should be in closer vicinity to each other. The heave amplitudes are low and the periods are up to 12 seconds long. Hence, the deviations are believed to be because of sensor offset errors. Results from the mathematical model shows more equal pressures when simulated. Together with the simulation and assumptions above it is therefore assumed that the pressures from the log data can be shifted in vertical direction to coincide with each other. Also, a phase shift between the pressures are expected due to inertia and flow resistance in the pipes. At first glance, it looks like there are no phase shift between the pressures in figure 4.3. It is expected that a phase shift should be visible between the plunger pressure and APV pressure. These two pressure are shifted to coincide and plotted in figure 4.4.

It is not very visible due to noisy signals, but at a closer look, one can see that the APV pressure lags a little bit behind the plunger pressure. This is shown in figure 4.5. As can also be seen, the APV pressure variation are slightly higher than for the plunger pressure. The calculated pressures are less noisy, and if plotted on top of the log data, the phase shift is more clearly visible between the two calculated pressures. This can be seen in figure 4.5. It is also clear from the calculations that the APV pressure will

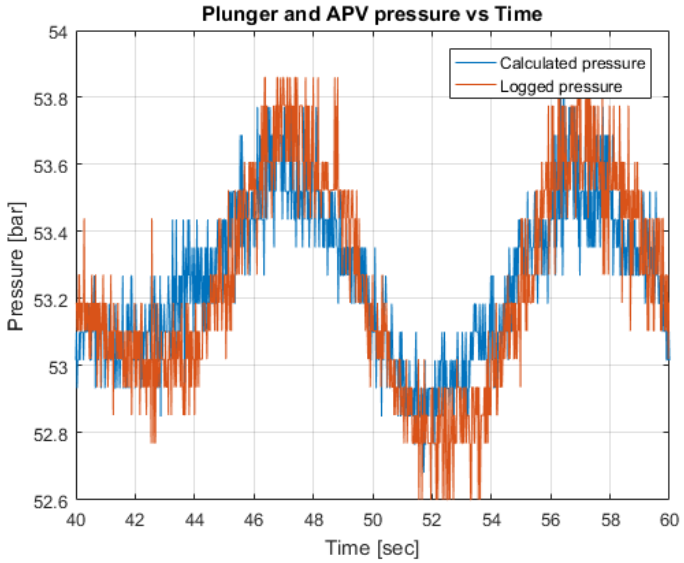

Figure 4.4: Logged plunger and APV pressure shifted in vertical direction to coincide

have a slightly higher pressure variation, which is in good accordance with the log data.

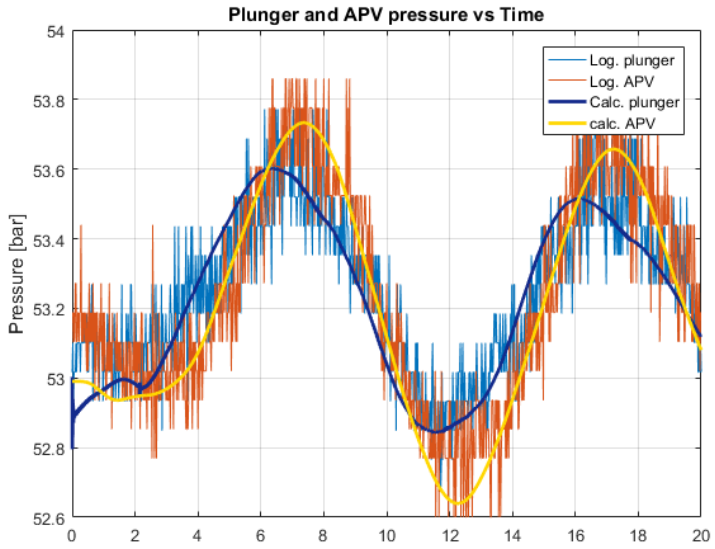

Figure 4.5: Calculated plunger and APV pressure together with logged pressures

4.2.1 Constant Temperature

Often, the energy balance is neglected and temperature is assumed constant when simulating fluid flow systems [20]. In fiugre 4.6, pressures with fixed temperature are compared to pressures with variable temperature. As can be seen from the plots, if temperature is held constant, the pressure will be lower than for pressures with variable temperature. This is expected, as pressure is proportional to temperature. From examination of the plots in figure 4.6, it is found that the deviation in pressure variation is in the region 20-30%. It should be noticed that this deviation is calculated in regards to pressure variation from the start pressure of around 53 bars, and *not* variation in regards to 0 bar.

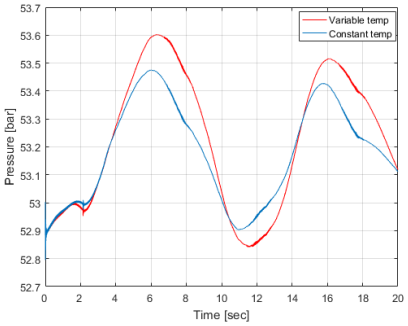

(a) Plunger pressure

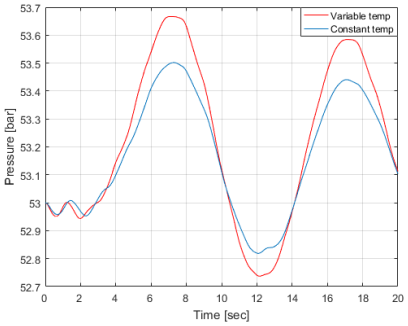

(b) Accumulator oil pressure

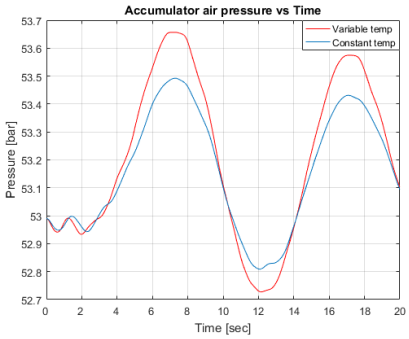

(c) Accumulator air pressure

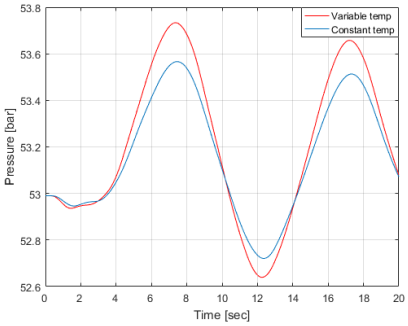

(d) APV pressure

Figure 4.6: Pressures with constant temperature compared to pressure with variable temperature

As a consequence of less pressure, there will be less force acting on the piston, leading to a greater piston stroke. This can can be seen in figure 4.7.

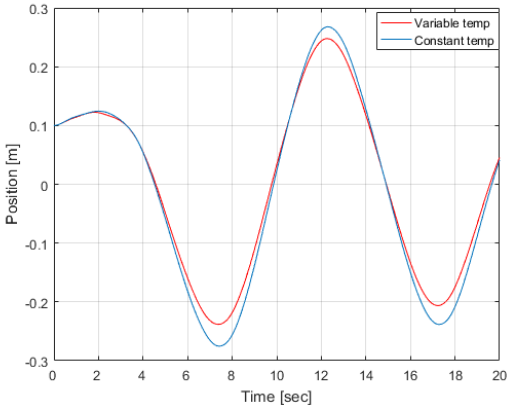

Figure 4.7: Cylinder position with constant temperature compared to position with variable temperature

4.2.2 Ideal gas

As stated in previous sections, the ideal gas law can predict behaviour of gases with reasonable accuracy for many cases. The compressibility factor, Z, is a measurement of how much a certain gas will deviate form the ideal gas. This can give a good indication on whether to use the ideal gas law, or if non-ideal equations should be used. Nitrogen has a critical pressure of 34 bar, and a critical temperature of 126.15 kelvin. For the specific case considered, the simulation is performed with a working pressure around 53 bar, and a temperature of 273.15 kelvin. This can be restated in terms of reduced pressure, p_R, and a reduced temperature, T_R:

$$p_R = \frac{p}{p_{cr}} = 1.55 \tag{4.2}$$

$$T_R = \frac{T}{T_{cr}} = 2.36 \tag{4.3}$$

For more details regarding critical and reduced properties, refer to section 2.2. From the chart in figure 2.6, one can see that this leads to a compressibility factor approximately equal to 0.96. The plots in figure 4.8 shows the pressures calculated with the ideal gas law.

As can be seen from the plots in figure 4.8, the ideal pressures are slightly higher compared to the pressures calculated with the Redlich-Kwong EOS.

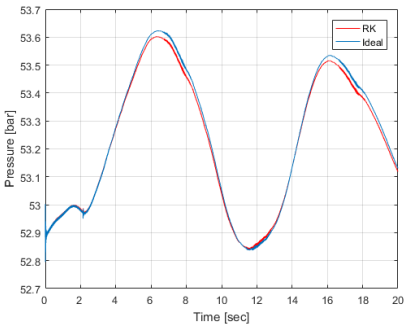

(a) Plunger pressure

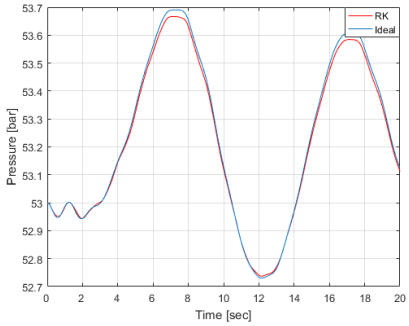

(b) Accumulator oil pressure

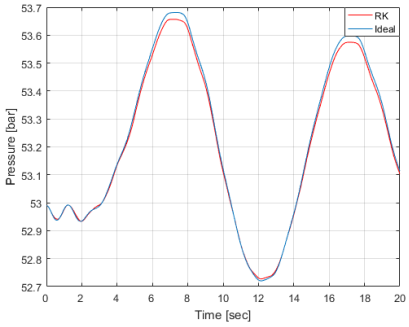

(c) Accumulator air pressure

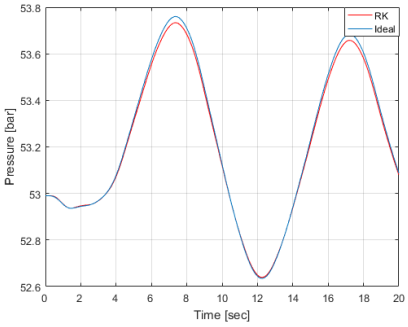

(d) APV pressure

Figure 4.8: Pressures CMC with constant temperature

The pressure variation in the accumulator, simulated with the Redlich-Kwong equation, is about 0.7 bar, while the pressure variation with ideal gas is approximately 0.73 bar. Compared to each other, this gives a difference of about 4%. As can be seen from these results, for a reduced pressure of 1.55 and reduced temperature of 2.36, the ideal gas law can be applied with a deviation of about 4% from the Redlich-Kwong equation. This is in good accordance with the compressibility chart.

To verify the equations behaviour compared to the compressibility chart, a simulation closer to the critical points is performed. This will not be representative for the physical system, but is merely done to validate the used equations to the compressibility chart. For this simulation, $p_R = 1.45$, and $T_R = 1.2$. From the chart, this gives a lower value for the compressibility factor, and the Redlich-Kwong pressure should be visibly lower than the ideal pressure. This simulation is showed in figure 4.9.
Reduced pressure of 1.42 gives a start pressure of approximately 48.3 bar. The pressure variation simulated with the Redlich-Kwong equation in figure 4.9a, gives a pressure variation of about 0.25 bar. The same simulation with

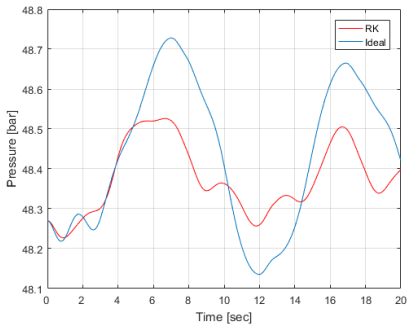

(a) Accumulator gas pressure near critical point for RK EOS and Ideal gas law

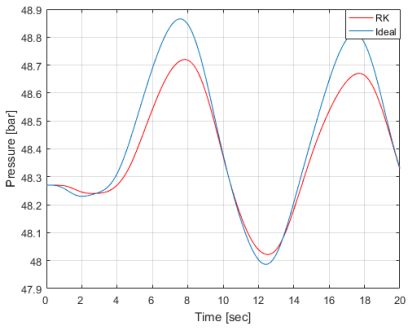

(b) APV pressure near critical point for RK EOS and Ideal gas law

Figure 4.9: Gas pressure for accumulator and APVs with RK EOS and ideal gas law

the assumption of ideal gas gives a pressure variation of approximately 0.5 bar. This is a doubled pressure variation compared to the Redlich-Kwong equation. The same behaviour can be seen in figure 4.9b for the APV pressure. The results, in regards to the compressibility chart, behaves as expected. It is therefore clear that, depending on desired accuracy of the simulation, the general compressibility chart should be used actively to decide which equation of state should be used for the simulations.

4.2.3 Higher Waves

To see how the model behaves at other conditions, a simulation with different wave amplitudes and periods are tested. Instead of using the logged data from the MRU, waves are generated in Matlab. For this simulation, the waves are set to have an amplitude of approximately 1.5 meters, and a period of 10 seconds. The reults can be seen in figure 4.10.
For this case, the pressure rise in the plunger cylinder is much higher than for previous cases. This is due to higher amplitude waves with shorter period than from the logged data. In fact, the waves are over a meter higher, leading to a longer piston stroke. This will cause a higher pressure in the plunger cylinder compared to the previous results. Notice that the pressures in the remaining volumes do not follow the pressure in the plunger cylinder as closely as before. As the pressure rise in the plunger cylinder is quite high, it follows that the flow out of the cylinder is also quite high. From the equations in chapter 3 it is clear that the losses through valves, and friction along pipes, will have more impact as the flow increases. This makes the pressure raise in the plunger cylinder higher, and the losses will work against the flow out of the cylinder to a greater extent.

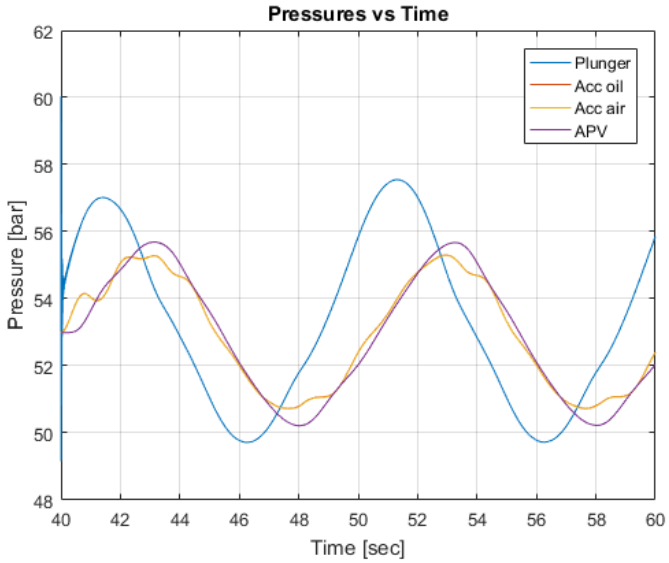

Figure 4.10: Pressure variation for higher waves

4.2.4 Isolation

In some cases it is desirable isolate the hydraulic system. This could be for testing of the active system, without interruption from the passive system, or also for testing of control system and software. Therefore, it is important that the compressibility of the hydraulic liquid is included. To verify the compressibility of the hydraulics, a simulation is performed where the isolation valve is closed. The simulation is conducted with the same conditions as in section 4.2.3, with a wave amplitude of 1.5 meter and a period of 10 seconds. The results are illustrated in figures 4.11 and 4.12.
In figure 4.11a, which shows the piston position relative to the cylinder, the effect of compressibility can be seen. This shows a movement of just above 2 mm. This deviation is so small that it is not possible to see in figure 4.11b, where the absolute position of the piston is plotted together with the MRU position. The small deviation from the MRU position is due to low compressibility of the liquid. As the hydraulic system is isolated, the pneumatic system is not damping any of the pressure forces. Therefore, a pressure rise of around 8-10 bar can be seen in figure 4.12, which is higher compared to the former simulations.

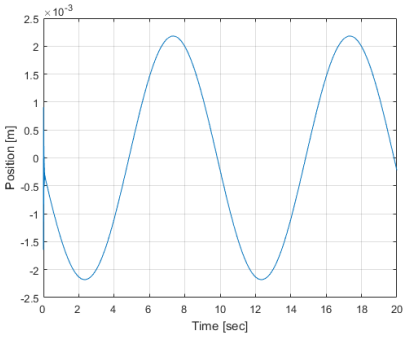

(a) Relative cylinder position

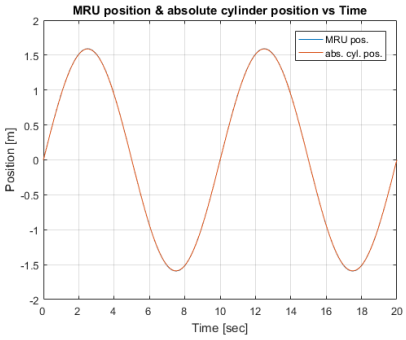

(b) Absolute cylinder position compared to MRU position

Figure 4.11: Relative and absolute cylinder position with isolation valve closed

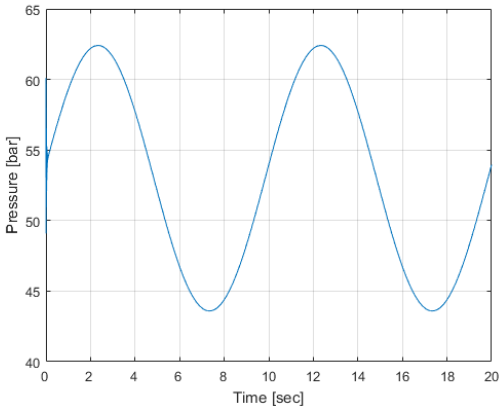

Figure 4.12: Pressure in plunger cylinder with isolation valve closed

Chapter 5

Conclusion and Further Work

5.1 Conclusion

In this thesis, a mathematical model for a hydro-pneumatic compensation system is proposed. The model is attempted to account for losses and phenomena that are often assumed to be of negligible contribution to the total system, and investigate its effect on the total system. The performance is verified against log data from actual processes and a discussion regarding importance of non-ideal behaviour is done.

From the simulation results, the general behaviour of the model is considered to be in good accordance with the log data. From the piston position plot, there are small deviations between logged piston position and simulated piston position, but in general the deviations are not excessive. The pressures, when plotted, also shows good behaviour in accordance with the given log data. It is expected that some offset errors are present in the logged data. When plotting pressures from the four volumes, they are behaving in the same fashion, but are gradually shifted in vertical direction to each other. As the amplitudes are relatively low, and the periods are up to 12 seconds long, it is expected that the pressures should be in closer vicinity to each other. It was therefore concluded that this might be due to offset errors in the sensors. To work around this problem, the pressures were shifted manually to a common point, where they seem to behave as expected. This can also be justified on the basis that all of the logged pressures are in accordance with simulated results from the model when the vertical shifting is done.

After the model was verified against log data, it was compared to simplified versions. This was done to investigate the importance of different things in

the model.

To investigate the importance of implementing a dynamic temperature equation, a comparison with the model under the assumption of constant temperature was done. It was seen that in general, assuming constant temperature leads to a decrease in pressure variation. As pressure is proportional to temperature, it was as expected that the pressure variation became smaller when the temperature variation was neglected. For the given conditions in sec 4.2.1, the temperature variation is about two degrees Celsius. As can be seen from figure 4.6, the deviation between the models are about 20-30%.

The impact of the Redlic-Kwong was investigated in the next simulation. It was found that under the given conditions, the ideal gas law was a predicting the pressures with only 4% deviation. As the deviation was this small, also the prediction of piston position was in near vicinity of the Redlich-Kwong predictions. It was concluded that the ideal gas could be applied without substantial loss in accuracy.
It was further done a simulation closer to the critical point of the gas, where, from the compressibility chart, the deviation is assumed to be higher. In this case, the deviation between the two gas equations was much higher. The ideal gas estimated a pressure variation of almost the double of the Redlich-Kwong equation. This is in accordance with the compressibility chart. It was therefore recommended to use the compressibility chart as a reference when choosing equation of state for future simulations.

The model was also tested for two different cases with higher waves. The first simulation was with the isolation valve open, while the second simulation was performed with the isolation valve closed.
With the isolation valve open, the pressure was significantly higher in the plunger cylinder compared to the other volumes. As the wave gets higher, the piston will have to travel a longer distance to compensate for the wave motions. This will lead to a higher pressure in the plunger cylinder due to a significantly lesser volume. From figure 4.10 one can notice that the pressures in the other volumes does not follow the pressure in the plunger cylinder as closely as the foregoing simulations. As the pressure in the plunger cylinder rises relatively quickly, it follows that the flow out of the cylinder is higher. From equations established in chapter 3, it is clear that the losses trough valves, and friction along pipes, will have a greater impact as flow increases. This makes the pressure rise higher in the plunger cylinder, as the losses will work against the flow out of the cylinder.

It was found that if the isolation valve is closed, the compensation will be almost zero. From the plot in figure 4.11a, it can be seen that the relative piston movement is about 2 mm. due to the compressibility of the hydraulic

oil. In figure 4.11b, one can not see a difference between the MRU position and cylinder absolute position due to the small relative movement of the plunger piston. As the pneumatic system is not providing any dampening, a substantial pressure rise can be seen in figure 4.12.

5.2 Furhter Work

The model seems to perform well compared to provided log data. But there are still some modifications and work which can be done.

To make the model more efficient, other solvers should be implemented. The Euler solver used in this thesis is known to be simple, but requires high sampling rate to give accurate results [21]. The author would suggest to implement a version of a Runge-Kutta solver to see how this affects the performance of the model.

As stated in the thesis, the flow to the force equalizers is neglected. It could be interesting to see how a separation of the gas in the gas piping would affect the dynamics of the total system.

Bibliography

[1] JK Woodacre, RJ Bauer, and RA Irani. A review of vertical motion heave compensation systems. *Ocean Engineering*, 104:140–154, 2015.

[2] Sten Magne Eng Jakobsen. Passive heave compensation of heavy modules. Master's thesis, University of Stavanger, Norway, 2008.

[3] Yunus A Cengel and Robert H Turner. *Fundamentals of thermal-fluid sciences*. McGraw-Hill, New York, NY, 3rd edition, 2008.

[4] Jose O Valderrama. The state of the cubic equations of state. *Industrial & engineering chemistry research*, 42(8):1603–1618, 2003.

[5] Witold Pawel Pawlus, Fred Liland, Nicolai Nilsen, Soren Oydna, Geir Hovland, Torstein Kurt Wroldsen, et al. Optimization of a high fidelity virtual model of a hydraulic hoisting system for real-time simulations. In *International Petroleum Technology Conference*. International Petroleum Technology Conference, 2014.

[6] J Bélanger, P Venne, and JN Paquin. The what, where and why of real-time simulation. *Planet RT*, 1(0):1, 2010.

[7] S Tanaka, Y Okada, and Y Ichikawa. Offshore drilling and production equipment. *Civil Engineering, Encyclopedia of Life Support Systems (EOLSS). Oxford: Eolss Publishers*, 2005.

[8] D. D. Boettner M. J. Moran, H. N. Shapiro and M. B Bailey. *Principles of Engineering Thermodynamics*. John Wiley & Sons, Hoboken, NJ, 7th edition, 2012.

[9] Sashay Ramdharee, Edison Muzenda, and Mohamed Belaid. A review of the equations of state and their applicability in phase equilibrium modeling. International Conference on Chemical and Environmental Engineering, 2013.

[10] Alf Kristian Gjerstad. *Simplified Flow Equations for Single-Phase non-Newtonian Fluids in Couette-Poiseuille Flow and in Pipes - For Dynamic Modeling of Surge and Swab Pressure in Oil Well Drilling Operations*. PhD thesis, UiS, 2014.

[11] Sigurd Skogestad. *Chemical and energy process engineering*. CRC press, 2008.

[12] Michael R Hansen and Torben O. Andersen. *Hydraulic Components and Systems*. University of Agder, 2006.

[13] Crane Co. Flow of fluids through valves, fittings and pipe. Technical report, New York, N.Y, 1982.

[14] J E Finnemore and J B Franzini. *Fluid Mechanics with Engineering Applications*. McGraw-Hill, New York, NY, 10th edition, 2002.

[15] Ajinkya A More. Analytical solutions for the colebrook and white equation and for pressure drop in ideal gas flow in pipes. *Chemical engineering science*, 61(16):5515–5519, 2006.

[16] Skjalg E Haaland. Simple and explicit formulas for the friction factor in turbulent pipe flow. *Journal of Fluids Engineering*, 105(1):89–90, 1983.

[17] R Darby and R P Chhabra. *Chemical Engineering Fluid Mechanics*. CRC Press, Boca Raton, FL, 3rd edition, 2016.

[18] Sashay Ramdharee, Edison Muzenda, and Mohamed Belaid. A review of the equations of state and their applicability in phase equilibrium modeling. International Conference on Chemical and Environmental Engineering, 2013.

[19] Bahman Zohuri and Patrick McDaniel. *Combined cycle driven efficiency for next generation nuclear power plants: An innovative design approach*. Springer, 1st edition, 2015.

[20] Saeed Farokhi. *Aircraft propulsion*. John Wiley & Sons, 2nd edition, 2014.

[21] Daniel Simon. *Fighter Aircraft Maneuver Limiting Using MPC: Theory and Application*, volume 1881. Linköping University Electronic Press, 2017.